

# Agent-based modeling of COVID-19 outbreaks for New York state, UK and Novosibirsk region

Olga Krivorotko<sup>a,b,\*</sup>, Mariia Sosnovskaia<sup>b</sup>, Ivan Vashchenko<sup>b</sup>, Cliff Kerr<sup>c</sup>,  
Daniel Lesnic<sup>d</sup>

<sup>a</sup>*Institute of Computational Mathematics and Mathematical Geophysics Siberian Branch of the Russian Academy of Sciences, 6 Prospect Akademika Lavrentieva Street, Novosibirsk, 630090, Russia;*

<sup>b</sup>*Novosibirsk State University, 2 Pirogova Street, Novosibirsk, 630090, Russia;*

<sup>c</sup>*Institute for Disease Modeling, Bill & Melinda Gates Foundation, Seattle, USA.*

<sup>d</sup>*University of Leeds, LS2 9JT, UK.*

---

## Abstract

This paper uses Covasim, an agent-based model (ABM) of COVID-19, to evaluate and scenarios of epidemic spread in New York State (USA), the UK, and the Novosibirsk region (Russia). Epidemiological parameters such as contagiousness (virus transmission rate), initial number of infected people, and probability of being tested depend on the region's demographic and geographical features, the containment measures introduced; they are calibrated to data about COVID-19 spread in the region of interest. At the first stage of our study, epidemiological data (numbers of people tested, diagnoses, critical cases, hospitalizations, and deaths) for each of the mentioned regions were analyzed. The data were characterized in terms of seasonality, stationarity, and dependency spaces, and were extrapolated using machine learning techniques to specify unknown epidemiological parameters of the model. At the second stage, the Optuna optimizer based on the tree Parzen estimation method for objective function minimization was applied to determine the model's unknown parameters. The model was validated with the historical data of 2020. The modeled results of COVID-19 spread in New York State, the UK and the Novosibirsk re-

---

\*Corresponding author

*Email addresses:* krivorotko.olya@mail.ru (Olga Krivorotko),  
m.sosnovskaya@g.nsu.ru (Mariia Sosnovskaia), i.vashchenko@g.nsu.ru (Ivan  
Vashchenko), ckerr@idmod.org (Cliff Kerr), D.Lesnic@leeds.ac.uk (Daniel Lesnic)

gion have demonstrated that if the level of testing and containment measures is preserved, the number of positive cases in New York State and the Novosibirsk region will remain the same during March of 2021, while in the UK it will reduce. Due to the features of the data for the Novosibirsk region (two datasets are characterized as stationary series with probability of 1), the forecast precision is relatively high for the number of hospitalizations, but is lower for new cases of COVID-19.

*Keywords:* epidemiology, agent-based modeling, COVID-19, interventions analysis, coronavirus data analysis, New York State, United Kingdom, Novosibirsk region, mathematical modeling, forecasting scenarios, reproduction number, optimization, OPTUNA software.

---

## 1. Introduction

In December 2019, the COVID-19 pandemic originated in the Wuhan province of China. Since that time, more than 130 million people in 192 countries have been infected with the disease, and more than 2.87 million people have died  
5 after getting infected. During the year 2020, mankind mobilized its resources to fight the pandemic. One of the useful tools in this struggle has been mathematical modeling that uses known historical data to study different scenarios of disease spread [1, 2].

The models including those for studying coronavirus infections can be di-  
10 vided into two groups: compartmental and agent-based models. In compartmental models, a population is divided into groups sharing similar features and interacting with one another following the mass action law. Agent-based models (ABMs), on the other hand, give each agent (people, social institutes, the state, etc.) a set of features and determines the way the agents interact from  
15 random graphs following disease spread principles. In other words, an agent's behavior is determined individually, and their joint behavior is described as the interaction of multiple agents (bottom-top approach). Unlike compartmental models, ABMs are capable of providing a detailed description of an epidemio-

logical situation, especially in a case of inaccurate and insufficient data. ABMs  
20 account for the stochastic nature of epidemic spread, makes it possible to estimate the likelihood of different epidemic scenarios, and allows one to evaluate the risks of unfavorable events occurring due to policy changes. The resulted data enable one to make conclusions about the duration, severity and scale of an epidemic, evaluate the efficacy of the preventive and quarantine measures,  
25 and assess its economic consequences.

During 2020, many models were developed to predict COVID-19 spread. In [3], both compartmental and agent-based models are presented to study mass face-mask wearing and predict its effect on COVID-19 spread. A graph-based ABM is suggested in [4]. The paper considers a small population of  
30 1000 agents and graphs of different kinds such as fully-connected, Barabasi-Albert, Watts-Strogatz ones, etc. Another approach to agents interactions is demonstrated in [5]. In this paper, agents are initialized in a 2D space (so-called mesh) to consider a distance between different agents, so such a factor as social distancing can be explicitly accounted for. However, this approach  
35 leads to excessive computation complexity, and for that reason, these models consider a small number of agents (up to 500).

Another important direction of modeling has been a comparison of containment measures and projecting the future for different scenarios. The paper published by Chang et al. [6] combines an epidemiological SEIR model and  
40 the hourly GPS data from the mobile phones of 98 million people in 10 US cities. The model predicted that closing of the most crowded public places such as restaurants and religious establishments would be a sufficient measure to contain the pandemic unlike unilateral measures to limit people's mobility. In [7], the authors offer an ABM using SEIR agents to model COVID-19 spread  
45 dynamics, where the agents imitate people, businesses and the government. Using the model, they have analyzed seven social-distancing scenarios having different epidemiological and economic effects. The paper has demonstrated that the so-called vertical isolation has no positive effect. In [8] macroeconomic epidemiological ABM been presented to study the economic effect COVID-19

50 would have in different scenarios of pandemic containment such as closing of educational and entertainment facilities. The model was calibrated using the statistical data on country's and business demography, households, employment, profits and wages in Germany.

It is noteworthy that data collecting and processing is a very important step  
55 in building an effective COVID-19 spread model. However, in the studies mentioned above data pre-processing for the modeled regions was not performed. Most of them concentrated on building the models and algorithms, whose parameters were considered known either from literature or from experts' estimations, so the issues of identifiability for unknown parameters have remained  
60 unresolved, as has the need of devising a regularization algorithm for solving the problem of epidemiological forecasting.

In this study, our focus is on the analysis of data, parameter identification, and regularization algorithms. However, it is a known fact that epidemics develop differently in different locations. To address this issue, in our study, the  
65 epidemiological situations in New York State (USA), the UK, and the Novosibirsk region (Russia) were compared and analyzed.

### 1.1. *New York State*

Nearly 2 million people were confirmed infected and more than 50000 people died by April 6, 2021 in NY State [9]. In NY State, the pandemic spread  
70 rapidly, reaching its peak in March-April of 2020 (see Section 2.1). The health-care system was overloaded in the very first months of the outbreak. Thanks to the containment measures introduced, the number of infected people reduced to a characteristic plateau that was followed by a second infection wave several months later.

### 75 1.2. *United Kingdom*

Another pandemic scenario was observed in the UK. After the first infection wave had been successfully suppressed by June, 2020, the second wave hit the country hard and, due to the B.1.1.7 SARS-CoV-2 variant, the number of

infected people increased 10 times compared to the first wave (see Section 2.3).

80 At the time of writing, this has reduced to 7000 cases a day, and the pandemic is on wane.

### 1.3. *Novosibirsk region*

The region's peculiar feature was the absence of the characteristic peaks that rather looked like plateaus (see Section 2.3), so the lockdown introduced  
85 in April 2020 had outlived its usefulness by the summer of 2020.

This study is organized as follows. First, open-source data of COVID-19 spread in New York State, the UK and the Novosibirsk region were processed and analyzed using the statistics and machine learning methods to find interdependencies, study seasonality and predict possible future dynamics (see  
90 Section 2). Second, we confirmed that the selected ABM met the identifiability condition such as being sensitive to data errors and capable of unambiguous determination of the unknown parameters of COVID-19 spread from additional measurements (Section 3.2). The obtained space of identifiable parameters was specified using the multilevel global-optimization method (Section  
95 4). Finally, scenarios of how the COVID-19 pandemic that could develop in New York State, the UK and the Novosibirsk region were assessed concerning available data and certain containment measures (Section 5).

## 2. **Data analysis**

Data analysis and data processing are important parts of forecasting modeling.  
100 eling. Before data processing begins, one has to understand the character of available data and determine their features. Collecting such daily indicators as the number of tests, diagnosed cases, ventilated COVID patients, etc. (see Table 1) helps to overview the general picture for a considered region, while anomalous time intervals may call for more scrupulous analysis.

Table 1: Indicators used in data analyses and their description.

Indicator	Description
New Tests	Number of performed tests
New Diagnoses	Number of diagnosed cases
New Deaths	Number of deaths related to a positive COVID-19 diagnosis
Num Critical	Number of ICU patients with suspected and positive COVID-19 diagnosis

105 2.1. New York State (USA)

To forecast the way the pandemic would develop, the data from the COVID Tracking Project’s website [11] were used. The site contains information for each state and for the country as a whole. The feature of the data in question is the method they calculate New Diagnoses: positive cases (confirmed plus probable) summing the total number of confirmed cases and the probable cases of COVID-19 reported by the state or territory, ideally per the “August 5, 2020 CSTE case definition”. Some states are following the older “April 5th, 2020 CSTE case definition” or using their own custom definitions. The latter method of data collection is more suitable for ABMs since it takes into account the percentage of infected people that may have been simply neglected.

We can consider the COVID-19 spread in New York State in more detail, using the epidemic time-series data. Any time series can be decomposed into the following three elements:

$$X(n) = T(n) + S(n) + N(n). \tag{1}$$

Here,  $X(n)$  is a time-series value,  $T(n)$  is the value of the underlying time-series component;  $S(n)$  is the value of a seasonality component,  $N(n)$  is the value of a noise component for the  $n$ -th day. When analyzing a time series, we

found it was most useful to analyze its trend, since this determines an indicator's behavior in time. For expansion by the expression 1, the Hodrick-Prescott filter was applied [12] (see result in Fig. 1).

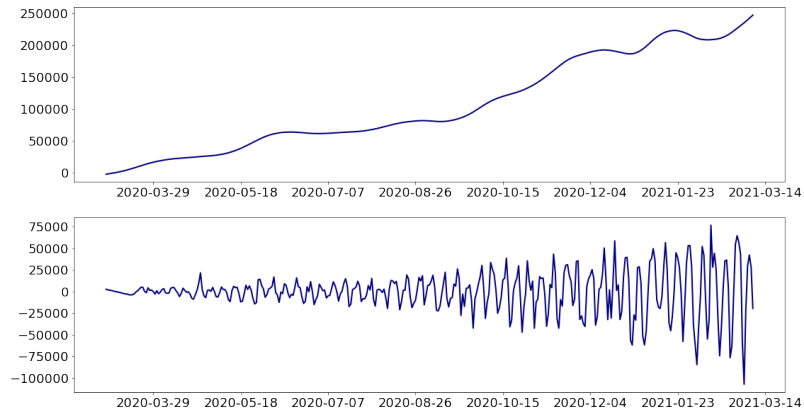


Figure 1: Graphs demonstrating the expansion results of the New Tests:  $T(n)$  (top) and  $S(n) + N(n)$  (bottom).

125 The non-smoothed graphs in Fig. 2 demonstrate widely dispersed points of statistics, so these data were smoothed before using them in the model because only the main trends of the curves were necessary for reaching an appropriate result. The graphs demonstrate certain periodicity that is known to be time series seasonality, which is clearly traced during summer in New Diagnoses.

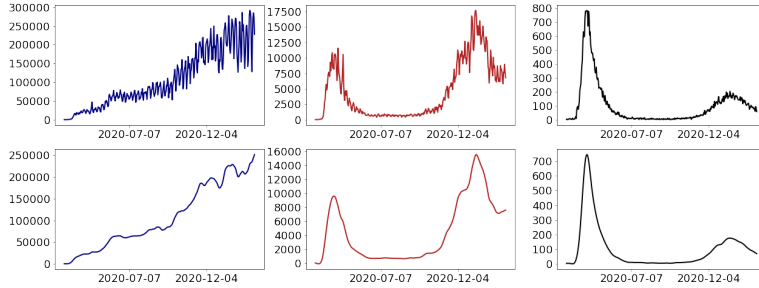


Figure 2: Graphs of COVID-19 spread in New York State (top line): the number of New Tests (left), New Diagnoses (middle) and New Deaths (right) and their smoothed curves (bottom line).

130 Now, let us consider the average fraction of tests for each day of the week that is calculated as:

$$w_i = \sum_{j=0}^N \frac{X(i + m \cdot j)}{S(i + m \cdot j)}.$$

Here,  $i$  is a week-day number,  $N$  is the number of full weeks within a considered time series,  $S(i + m \cdot j)$  is the cumulative sum of the New Tests performed within a week corresponding to index  $j$ ,  $m = 7$ . The results can be seen in  
 135 Table 2. It is apparent that the number of tests tends to its minimum for Mondays and Sundays and reaches its maximum on Fridays and Saturdays, which exemplifies the seasonality (i.e., periodicity) of the considered time series.



Table 2: Average fraction from the number of tests and its daily distribution for a whole statistics-gathering period (NY State).

Days of the week	Average fraction
Monday	0.113654
Tuesday	0.127697
Wednesday	0.134512
Thursday	0.155779
Friday	0.162017
Saturday	0.163702
Sunday	0.142640

COVID-19 pandemic data analysis has shown that there is a dependence between New Tests and New Diagnoses datasets for different regions. In such cases, the behavior of the second indicator is partly determined by that of the first. As a matter of fact, the last day of the week does not mean an abrupt increase in the number of the infected only because it is Friday. However, more people get tested on Friday, so the number of positive tests may increase. For that reason, analyzing the links between the number of infected people and that of new tests becomes crucial. For a proper understanding of the situation, it is not New Diagnoses, but their fraction from the number of New Tests that we want to know. After all, if one tested every person in a region, they would immediately indicate every one infected and their indicator would increase abruptly while their percentage would remain the same. Based on this fact, one can derive a time series that describes the percentage of newly tested people with either positive or potentially positive COVID-19 test.

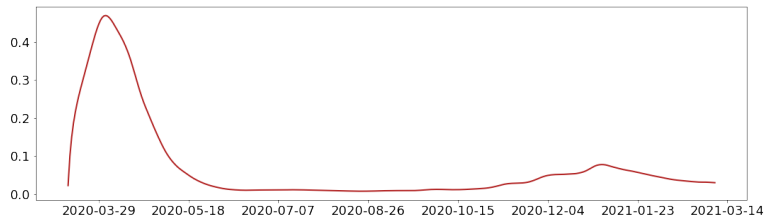


Figure 3: Fraction of New Diagnoses from New Tests in NY State.

Figure 3 shows that the ratio reached its peak in April 2020 and later started to reduce due to an increased number of tests. In autumn, the second pandemic wave began, so the number of daily confirmed cases increased (see Fig. 2), but the ratio between New Diagnoses and New Tests remained at a low level. This implies that testing behavior (i.e., the probability of testing with or without COVID-19 symptoms) did not change. The relatively few number of deaths over this period was due to the epidemic primarily spreading among younger age groups (see Fig. 2).

To confirm change in testing during autumn and winter, the MACD indicator [13] was used, whose histogram tracks a function's rise and fall (in our case it was the rise of New Tests). The graph demonstrates that the MACD indicator increased significantly over this period (see Fig. 4).

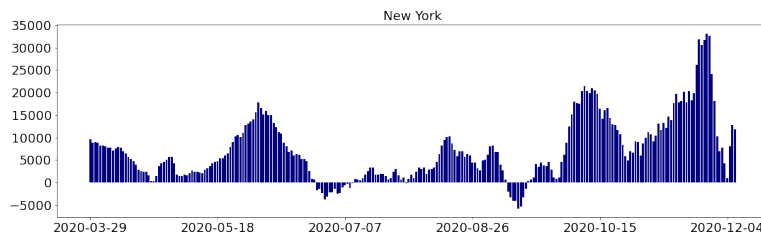


Figure 4: MACD-indicator of the New Tests in NY State.

### 2.1.1. Seasonality

165 The above-mentioned term “seasonality” refers to the periodic fluctuations observed in time series. In other words, if one takes a time-series space and overlaps it against a neighboring space of the same size, their profiles are going to coincide (or differ by a constant). The peak absolute values will correlate with the same time points calculated from the beginning of the space. As for  
170 our COVID-19 data, their seasonality can be traced in the New Tests indicator, which has its logic since collecting this statistics involves as a human factor as the features of the healthcare system. The seasonality of a time series makes it possible to forecast the series behavior relative to some average value.

Seasonality is commonly determined with an autocorrelation function (ACF). For a discrete process  $X(1), X(2), \dots, X(n)$  its formula is written as:

$$R(n) = \frac{1}{(M - n) \cdot \sigma^2} \sum_{t=1}^{M-n} (X(t) - \mu)(X(t + n) - \mu).$$

Here  $\sigma$  is the standard deviation of a discrete process  $X$ ,  $\mu$  is its average value,  
175  $M$  and  $n$  are positive integers. Besides, to analyze time-series seasonality, a partial correlation (PACF) was applied that removed the linear dependence between shifted time series.

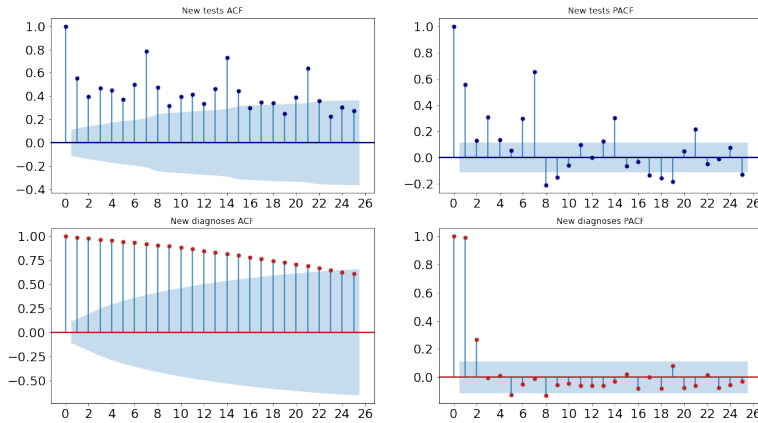


Figure 5: Graphical results of applying ACF (left) and PACF (right) to New Tests (top) and New Diagnoses (bottom) in NY State.

The results confirmed New Tests really had weekly seasonality (7, 14 and 21st days), while the New Diagnoses did not possess this property (see Fig. 5).

180 2.1.2. *New Tests/New Diagnoses interrelation*

We have also considered a percentage change for any current moment in relation to the same moment a week before:

$$pc(n) = \frac{X_{smoothed}(n)}{X_{smoothed}(n-7)} - 1.$$

This statistic demonstrates by how much an average indicator has changed in fractions compared to a previous week. If compared for weekdays, the results become smoother and easier to interpret.

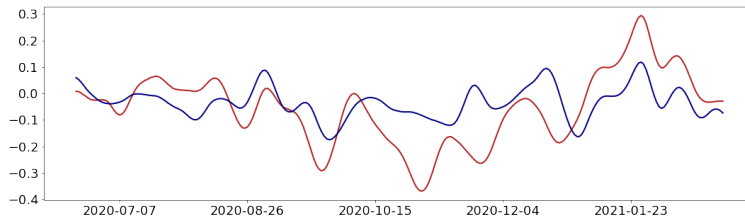


Figure 6: New Diagnoses percent change (red line) and New Tests percent change (blue line) time-series graphs in NY State.

The two time series in Fig. 6 have spaces where their trajectories almost  
 185 match. In other words, the percent change of one indicator differs from that  
 of the other one by a constant. In terms of tested/infected ratio, such spaces  
 confirm that within this period, the number of infected people grew owing to  
 the increased number of tests and not to a worsening pandemic situation in the  
 region.

190 For more specific analysis, a window of 28 days was correlated with the  
 previous 28 days for every day in the window (see Fig. 7).

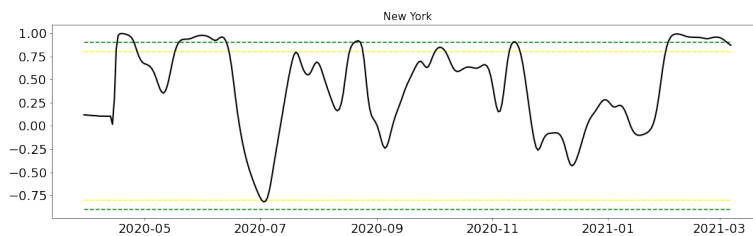


Figure 7: New Diagnoses percent change and New Tests percent change correlations within a 28-day backward window with  $|0.8|$  and  $|0.9|$  correlation's threshold lines for NY state.

In statistics, a significant linear dependence occurs when the absolute correlation value exceeds 0.8. If it exceeds 0.9, it means there is a strong dependence between two indicators. In NY State, with some deviations, New Diagnoses

195 strongly depended on New Tests. The deviations mean the pandemic develops following its own scenario. For instance, in the end of May and the beginning of June, the correlation coefficient exceeded 0.8 within a 28-day backward window when the first pandemic wave in the region was considered defeated and reached the so-called plateau that lasted till October when the second correlation took place and the second pandemic wave began, which means the  
 200 second wave might have been triggered by the abrupt increase of New Tests. However, the correlation coefficient got back to almost zero by December, indicating that the rise and fall of New Diagnoses did not correlate with New Tests, so the pandemic in the region at that time spread or reduced (depending on  
 205 graph direction). In February and March, the correlation became very close to one, meaning the number of infected people depended only on a New Tests.

## 2.2. Novosibirsk region

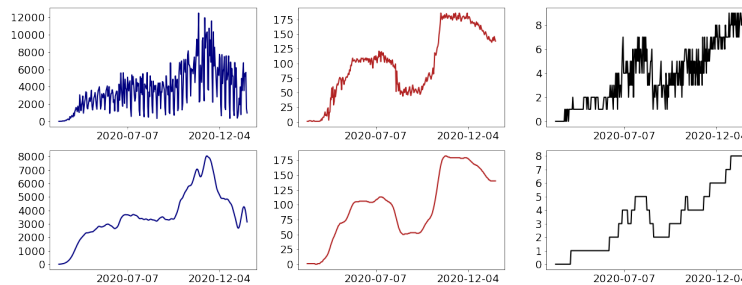


Figure 8: COVID-19 spread graphs for the Novosibirsk region (top line): New Tests (left), New Diagnoses (middle) and New Deaths (right) and their smoothed curves (bottom line).

The data (see Fig. 8) for our research were taken from the RBC website that published the daily statistics of COVID-19 spread in the Novosibirsk region  
 210 (the used data are given in Table 1). In March and May of 2020, these data had a significant number of gaps. For instance, the statistic on the number of performed tests was available only starting April 25, 2020, as the other statistics were accumulated starting March 17, 2020. For that reason, the New Tests was

extrapolated in relation to the abrupt increase in the number of New Diagnoses  
 215 starting April 6, 2020. For filling the gaps, the following backward extrapolation  
 algorithm was iterated:

$$X(n) = \frac{1}{m} \sum_{j=1}^m X(i+j) \cdot C^n + E(n), \quad i = L, \dots, 0.$$

Here,  $X(n)$  is the value of a time series of the  $n$ -th day;  $m = 7$ ,  $C = 1.03$ ,  $L$   
 is the number of gaps to be extrapolated;  $E(n)$  is a random value of normal  
 distribution, i.e.  $E(n) \in \mathcal{N}(0, \frac{X(n)}{3})$ . The extrapolation result for New Tests can  
 220 be seen in Fig. 9.

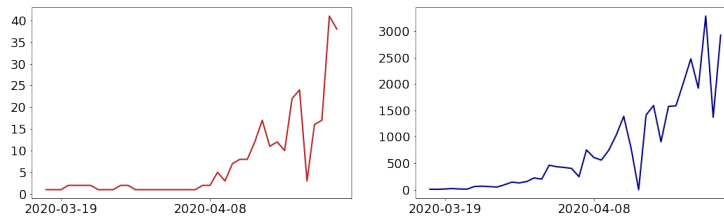


Figure 9: Backward extrapolation results for the New Tests (right) compared with the actual values  
 of New Diagnoses time series in the Novosibirsk region (left).

### 2.2.1. Seasonality

Here, the approach similar to that applied for the NY State data was im-  
 plemented to calculate the ACF and PACF for several time series (see Fig. 10),  
 together with the fraction of tests performed for every day of the week (see  
 225 Table 3).

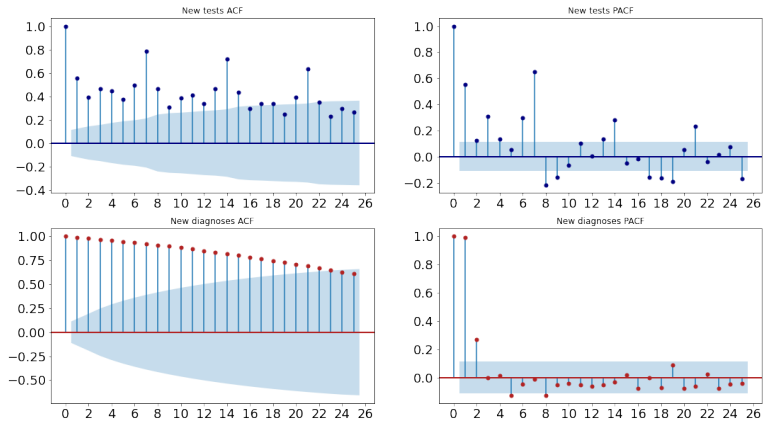


Figure 10: Graphical results of applying ACF (left) PACF (right) to the New Tests (top) and New Diagnoses (bottom) in the Novosibirsk region.

Table 3: Average fraction from the number of tests and its daily distribution for a whole statistics-gathering period in the Novosibirsk region.

Week days	Average fraction
Monday	0.064055
Tuesday	0.176845
Wednesday	0.148333
Thursday	0.161924
Friday	0.162173
Saturday	0.183951
Sunday	0.075146

As can be seen from Fig. 10, both functions confirmed the seasonality of New Tests with the duration of the season to be one week. As it has been discussed earlier, for this indicator this is absolutely normal. Table 3 demonstrates that the lowest fraction of tests was registered on Sunday and Monday, and the



230 highest one – on Tuesday and Saturday.

### 2.2.2. Stationarity

A time series is regarded as stationary (or weakly stationary) if its expected value and variance are time-independent, and its autocorrelation function depends only on a difference of neighboring values. Let us consider two time series for the New Diagnoses: from May 29 to July 1 and from October 24 to December 7 (see Fig. 8). Having applied the augmented Dickey-Fuller test, whose zero hypothesis is non-stationary time series (Unit root test), we find that this hypothesis can be rejected for both time series intervals, since their p-values are 0.0 and 0.001, respectively. If time series are stationary, the considered data sets can probably be interpreted as a normal noise. Table 4 demonstrates the results of two statistical tests to verify the normality of the considered time series.

Table 4: Results of the two statistical tests, whose zero hypothesis is the normal distribution of two stationary parts of New Diagnoses.

Time interval	Kolmogorov-Smirnov test ( $p$ -value)	D'Agostino-Pearson test ( $p$ -value)
29.05.2020 - 1.07.2020	0.3842	0.1827
24.10.2020 - 7.12.2020	0.573	0.8193

According to the test results, the null hypothesis of the normality of the two areas is not rejected. However, due to the small number of observations, it is equally impossible to assert that the values in the selected areas are normally distributed.

### 2.2.3. New Tests/New Diagnoses interrelation

Calculated New Diagnoses and New Tests percent change correlations (see Fig. 11) showed there was not even a single window of 28 days with a significant New Tests/New Diagnoses linear dependence. In the middle of June, a negative correlation peak was observed confirming the “more tests less positive

cases” tendency lasting from the end of June to the beginning of July. Another interesting fact was the New Diagnoses, percentage that plummeted in August while New Tests remained at the same level.

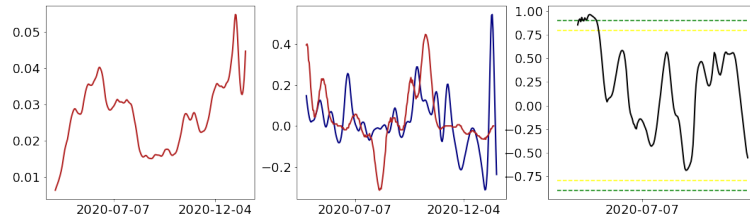


Figure 11: New Diagnoses to New Tests ratio (left); New Diagnoses (red) percent change and New Tests (blue) percent change (center) and their correlations within a 28-day backward window (right) with  $|0.8|$  and  $|0.9|$  correlation’s threshold lines for the Novosibirsk region.

### 2.3. United Kingdom

255 To analyze COVID-19 spread in the UK, the data accumulated on an official government web portal were used [15].

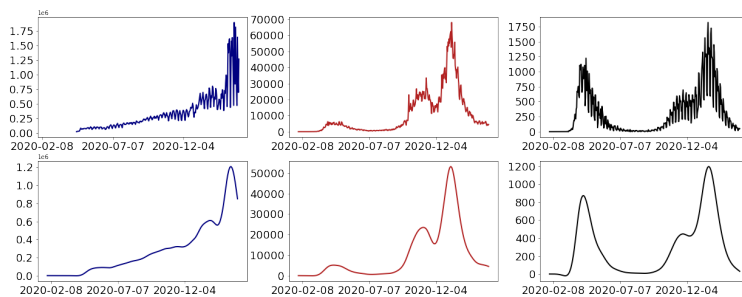


Figure 12: COVID-19 spread graphs in the UK (top line): New Tests (left), New Diagnoses (middle), New Deaths (right) and their smoothed curves (bottom line).

Fig. 12 shows two infection waves: spring (from 2020.03.09 to 2020.06.01) and fall (from 2020.09.01 to 2021.03.01) ones. The standard deviation of the

time series for the second wave was much bigger than for the first one. For that  
 260 reason, the standard deviation values were considered for three independent  
 time series of New Diagnoses and New Tests (see Table 5). The data for NY State  
 (NY) and the Novosibirsk region (NSK) are put in the table for comparison.

Table 5: Standard deviation values for particular New Diagnoses and New Tests time series in the UK, NY State and the Novosibirsk region.

Indicator	First	Second	Third	Fourth
(UK) New Tests std	10626.7	16613.8	77382.5	...
(UK) New Diagnoses std	455.8	201.1	5727.2	...
(NY) New Tests std	5636.6	9543.9	31127	...
(NY) New Diagnoses std	1137	114.2	1144	...
(NSK) New Tests std	765.2	1271.2	1596	2492
(NSK) New Diagnoses std	7	4.6	7	6

Unfortunately, the data did not allow us to conclude what was the exact  
 reason for the second wave's higher variance. It could have been the week  
 265 variance of New Tests or something else since, in the UK, they started to register  
 the number of tests only on 2020.04.21. All we know is the standard deviation  
 of New Diagnoses increased with time as well as the variance of New Tests.  
 However, both in NY State and the Novosibirsk region, despite the growing  
 variance of New Tests, the standard deviation value of New Diagnoses remained  
 270 at the same level.

### 2.3.1. Seasonality

The ACF and PACF applied to the New Diagnoses and New Tests time series  
 and the fractions of tests calculated for every day of the week demonstrated the  
 weekly seasonality of New Tests confirmed by ACF (see Fig. 13 and Table 6).  
 275 However, no significant PACF delays were observed. Comparing the results  
 obtained with those from NY State and the Novosibirsk region demonstrated  
 the absence of linear dependence did not affect the time series's seasonality.

However, a different situation was observed in the UK.

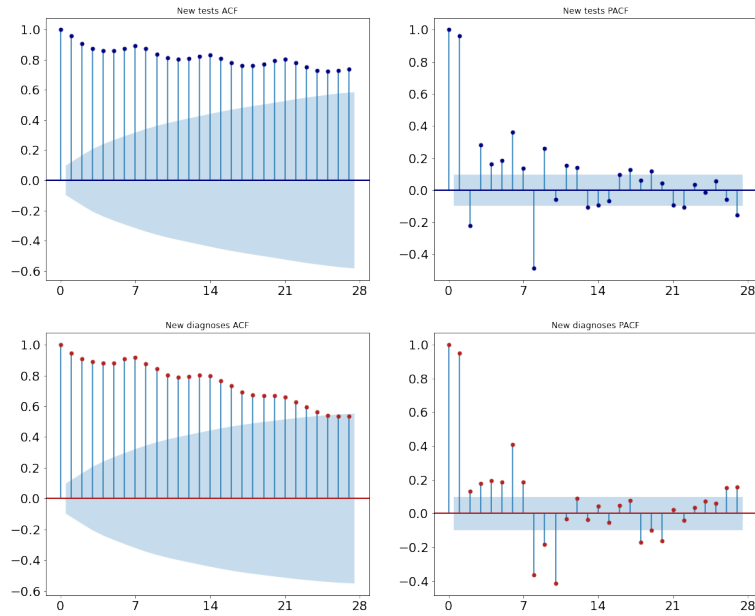


Figure 13: Graphical results of applying ACF (left) and PACF (right) to New Tests (top) and New Diagnoses (bottom) for the UK.

Table 6: Average fraction from the number of tests and its daily distribution for a whole statistics-gathering period in the UK.

Days of the week	Average fraction
Monday	0.125222
Tuesday	0.135905
Wednesday	0.159167
Thursday	0.166208
Friday	0.157837
Saturday	0.131992
Sunday	0.123668

In the next section, an approach to forecasting the New Tests time series will be demonstrated. The approach relies upon several techniques, including SARIMA, an algorithm requiring a significant correlation for the seasonal delays (7, 14, 21, etc.) of a single parameter.

#### 2.4. Forecasting New Tests

To draw forecast curves while modeling, one has to predict a number of certain statistical data sets that are used as input parameters. In our model, such a data set was the New Tests performed in the region since this indicator did not depend on the others and had the highest value of seasonality that determined the seasonality of the other indicators.

The first model considered for forecast purposes was SARIMA [16], a modification of ARIMA [17] (AutoRegressive Integrated Moving Average), which is able to support time-series data sets with a seasonal component. ARIMA is an extension of the ARMA models for non-stationary time series that can be converted into stationary ones through differencing of a certain order from an initial time series (so-called integrated or differential-stationary time series).

For a non-stationary time series  $X(n)$ , the  $ARIMA(p, d, q)$  model is written

as:

$$\Delta^d X(n) = c + \sum_{i=1}^p a_i \Delta^d X(n-i) + \sum_{j=1}^p b_j \epsilon(n-j) + \epsilon(n).$$

295 Here,  $\epsilon(n)$  is a stationary time series of white noise;  $c, a_i, b_j$  – model parameters;  $\Delta^d$  – difference operator of a time series of order  $d$  (sequential taking of  $d$  times of first-order differences: firstly, from a time series, then from obtained first-order differences, then from second-order differences and so on).

Parameters  $p, d, q$  and  $P, D, Q$  are determined through cross-validating  
300 minimization of the AIC-metrics. Here,  $p$  is the number of the last non-seasonal delay with significant PACF;  $P$  is the number of the last seasonal delay with significant PACF;  $q$  is the number of the last non-seasonal delay with significant ACF;  $Q$  is the number of the last seasonal delay with significant ACF;  $d$  is a differentiation order with 1-day delay,  $D$  is a seasonal differentiation order with 7-day delay. The ARIMA model is based on the following idea: one  
305 builds a model from the differences of a value for  $d$  sequential periods to obtain a stationary process. In a general case, the difference order is limited to  $d = 2$ , since taking the second-order differences allows converting almost any non-stationary data series into stationary ones.

310 As for the time-series forecast, the following algorithm was applied:

1. Applying the Box-Cox transformation [18] to reduce the variance.
2. Calculating the first-order seasonal difference (7-day shift).
3. Calculating the difference (1-day shift) of the series obtained at step 2.
4. Applying the Dickey-Fuller criterion to verify the stationarity of the series  
315 obtained at step 3.
5. Passing the hyperparameters corresponding to the actions performed and selecting other ones using the minimized Akaike information criterion. As data, the series from step 1 is passed.
6. The model with adjusted hyperparameters was used for forecasting. The  
320 obtained results were treated using the inverted Box-Cox transform.

The second model considered for the forecast was Holt-Winters [19], which provides triple exponential smoothing of a time series. The idea behind the

model is to break a time series into such components as a level, trend and seasonality. The last component explains repeating fluctuations around the level and the trend and is characterized by its duration, i.e. a period after which a fluctuation repeats itself. In this approach, each observation has its own component, e.g. if a season's duration is 7 days, there are 7 seasonal components, one for every day of the week.

To build the model, parameters  $\alpha$ ,  $\beta$  and  $\gamma$  had to be determined.  $\alpha$  is responsible for smoothing the series around the trend,  $\beta$  is for smoothing the trend itself,  $\gamma$  is the seasonality component. Minimizing mean absolute error (MAE) through time-series cross-validation, we selected the model's optimal parameters (iterative three-parameter random search).

To extrapolate the New Tests time series from the Novosibirsk region, in addition to the models described above, a linear regression model was used for comparative analysis. In this respect, for different time intervals, SARIMA's forecast results were on average not better but more stable than those produced by the other models (see Fig. 14).

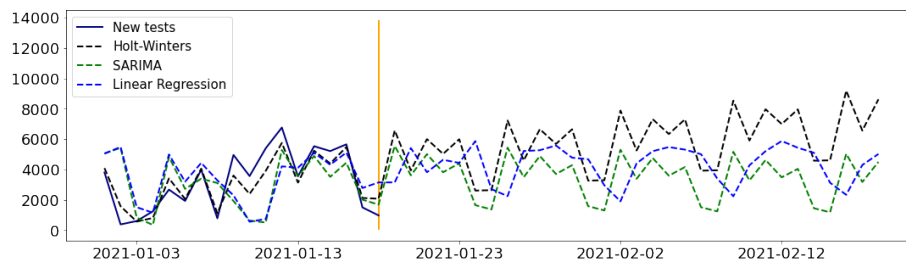


Figure 14: Monthly forecast results for the New Tests time series (dark blue line) for 2021.01.18 obtained using the Holt-Winters (black dashed line), linear regression (blue dashed line) and SARIMA (green dashed line) models for the data from the Novosibirsk region.

Table 7: Mean Absolute Error (MAE) between the New Tests time series and a corresponding prediction (from May 5, 2020 to January 18, 2020).

Forecast model	MAE
Holt-Winters model	1646.49
SARIMA model	1454.73
Linear Regression model	1586.34

As a result, the SARIMA forecast gave the lowest MAE (see Table 7). This  
340 algorithm also produced the most accurate seasonality and time-series autore-  
gression. For that reason, a decision was made to use SARIMA for forecasting  
the future values of New Tests.

### 3. Agent-based mathematical model

This section presents the ABM devised to describe COVID-19 spread and  
345 formulates a problem to identify (calibrate) the model's unknown parameters  
as objective functional minimization. It also presents a scheme for automatic  
calibration of the parameters for time intervals exemplified by the number of  
infected people in the Novosibirsk region.

#### 3.1. ABM formulation

350 Within the framework of this research, stochastic ABMs for New York State,  
the United Kingdom and the Novosibirsk region were devised. They were  
built using the Covasim [20]. This package had been utilized to predict the  
number of infected, dead and hospitalized people in the State of Oregon and  
become one of the tools to make decisions about whether to relax or escalate  
355 COVID-19 containment measures [21, 22]. This library is written in Python  
to study non-trivial COVID-19 dynamics. Its general algorithm is as follows:  
after all necessary parameters and statistical data are uploaded, the package  
creates an artificial population with account for age distribution. The model's



agent is a person in a particular region. Then, the agents are united into con-  
360 tact networks and the integration loop begins. At every time step (1 day), an  
agent's status is updated in relation to its contact network and the contain-  
ment measures relevant for this interval (self-isolation; closed access to public  
places; wearing face masks, etc.). The agents can interact with one another in  
particular networks. Depending on the network's structure, both full and ran-  
365 dom connectivity graphs are built for an agent to figure out how the infection  
spreads. The average number of daily contacts is different for every agent and  
every network. At any time moment, the agents distributed by their age (bins  
of 0-9, 10-19, ..., 90+) are found in their given state (see fig. 16). Our ABM also  
accounted for tested agents according to the data on COVID-19 tests performed  
370 in the Novosibirsk region. More details about the structure of Covasim-based  
ABMs, their parameters and realization methods can be found in [23].

Every agent has their set of properties and characteristics that can be di-  
vided into 2 groups: constant (belong to each particular agent and do not  
change while modeling) and time-dependent.

### 375 3.1.1. *Time-independent agent characteristics*

- Age( $t^*$ ). All the agents are subdivided into age groups of 10 years (0-9  
years, 10-19, ..., 90+. The age distribution depends on the demographic  
situation in a studied region.
- Social status (determined by an agent's age  $t^*$ ). Depending on their age,  
380 agents contact one another in contact networks. All agents have contacts  
in households and public places. Agents of 6-21 years old can also have  
contacts in educational institutions with agents of their age. Agents of  
22-65 years old contact at work (see Fig. 15). Depending on a contact's  
structure, the transmission parameter  $\beta$  is multiplied by corresponding  
385 constant  $w_\beta$  ( $w_\beta = 3$  for households, 0.6 – for educational institutions,  
0.3 – for public places), i.e. the likelihood of virus transfer is different for  
every network.

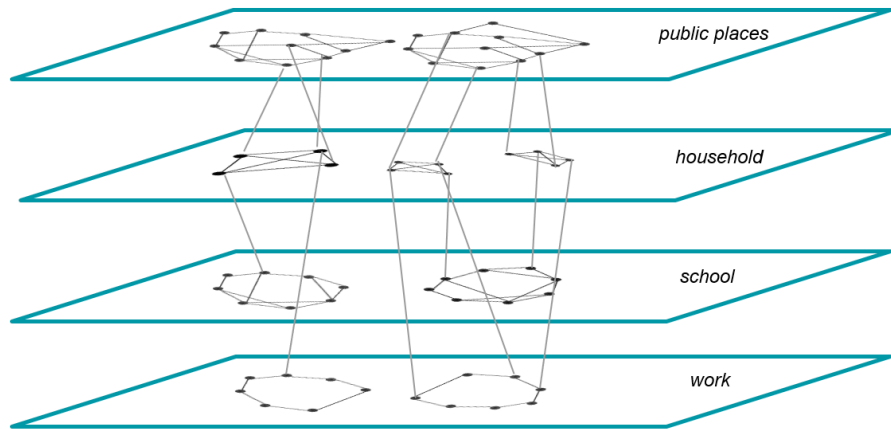


Figure 15: Agent contacts layers and their interactions in the COVID-19 spread ABM.

- Likelihood of disease progression (determined by an agent's age  $t^*$ ). These parameters determine disease progression (see Fig. 16). Their description is given in Table 8.

390

Table 8: Parameters of disease progression probability.

Parameter	Description
$p_{sym}(t^*)$	Probability of developing symptoms
$p_{sev}(t^*)$	Probability of developing severe symptoms (requires hospitalization)
$p_{crit}(t^*)$	Probability of critical condition (requires ICU)
$p_{death}(t^*)$	Probability of death

### 3.1.2. Time-dependent agent characteristics

- Agent's epidemiological status. Each agent may have one of the 10 stages of the disease (Fig. 16)  $\vec{X} = (S, E, I, A, Y, M, H, C, R, D)$ .
- Agent's chance to be tested for COVID-19 ( $\tilde{p}(X(t))$ ) that is determined by the agent's epidemiological status. The agents are tested daily, the

395

number of tests corresponds to the statistical data obtained in a region. At every modeling step, the tests are distributed across the population, the agents whose status is marked with an orange frame in a Fig. 16 can be given a positive result. The agents whose test is recognized as positive are marked as “confirmed” and included in New Diagnoses. The model assumes that the likelihood for an agent to be tested as a symptomatic carrier is higher and this chance ratio is controlled by parameter  $\tilde{p}(X(t))$  at is restored from solving the inverse problem (see the next section).

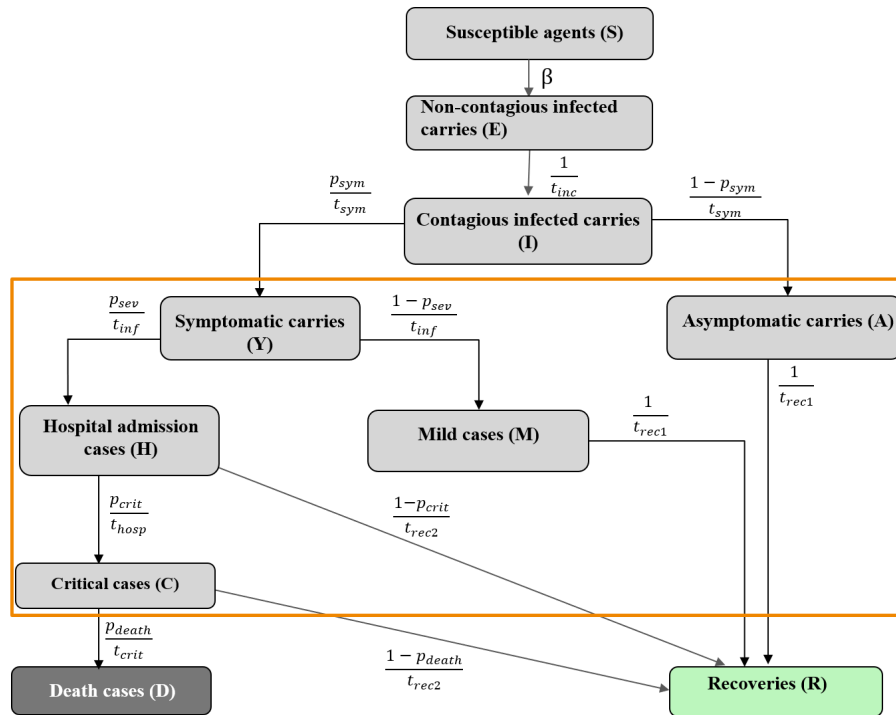


Figure 16: Agent state transition diagram in Covasim that is based on a SEIR-type compartment model. The orange frame marks those agent states that can give positive COVID-19 tests.

### 3.2. Parameter identification problem

The ABM developed was also characterized by unknown parameters vector  $\vec{q}$ . To specify the model’s parameters a variational inverse problem formulation

was performed to minimize the misfit function:

$$J(\vec{q}) = \sum_s \sum_{t_i=1}^T \frac{|X_d^s(t_i) - X_m^s(t_i, \vec{q})|}{M_s}. \quad (2)$$

405 Here,  $s$  is the statistics used for comparison, e.g. New Diagnoses, New Deaths, etc.;  $X_d^s(t_i)$  and  $X_m^s(t_i, \vec{q})$  are daily statistical and model data for statistics  $s$ ;  $T$  – the number of modeled days,  $M_s = \max_{t_i}\{X_d^s(t_i)\}$  is a normalising term.

### 3.3. Automatic parameter calibration

The model assumed that parameter  $\beta$  was a piece-wise constant, so the  
 410 days of change and new values were determined by parameters  $\vec{\beta}_d$  and  $\vec{\beta}_c$ .  
 The longer was a considered time interval, the more unknown parameters it  
 included. Since every launch of the model's calibration algorithm was rather  
 time-consuming, the time interval in question was divided into periods of 1  
 month. For example, for NY State the first period was 2020.03-02 - 2020.04.01,  
 415 the second – 2020.04.02 - 2020.05.0; for the UK – 2020.02.07 - 2020.03.08 and  
 2020.03.09 - 2020.04.07; for the Novosibirsk region - 2020.03.12 - 2020.04.11 and  
 2020.04.12 - 2020.05.11 etc.

Each period was sequentially calibrated, so the parameters restored at a  
 previous step were used in the following iteration of the optimization algo-  
 rithm. Thus, for the initial period considered the unknown parameter vector  
 was

$$\vec{q}_1 = (E(0), \beta, \beta_d(1), \beta_c(1), \tilde{p}(X)),$$

where  $E(0)$  is the initial number of infected agents,  $\beta$  is a contagiousness pa-  
 rameter value,  $\beta_d(1)$  is the day parameter  $\beta$  changes,  $\beta_c(1)$  is the value by  
 which parameter  $\beta$  changes on day  $\beta_d$ ,  $\tilde{p}(X)$  is a test level parameter in relation  
 to statistical data. For all the following periods (second, third, etc.):

$$\vec{q}_i = (\beta_d(i), \beta_c(i)).$$

Figure 17 displays a phased restoration of the vector of unknown parame-  
 ters  $\vec{q}$  for the Novosibirsk region exemplified by 4 out of 13 interim calibration  
 420 periods.

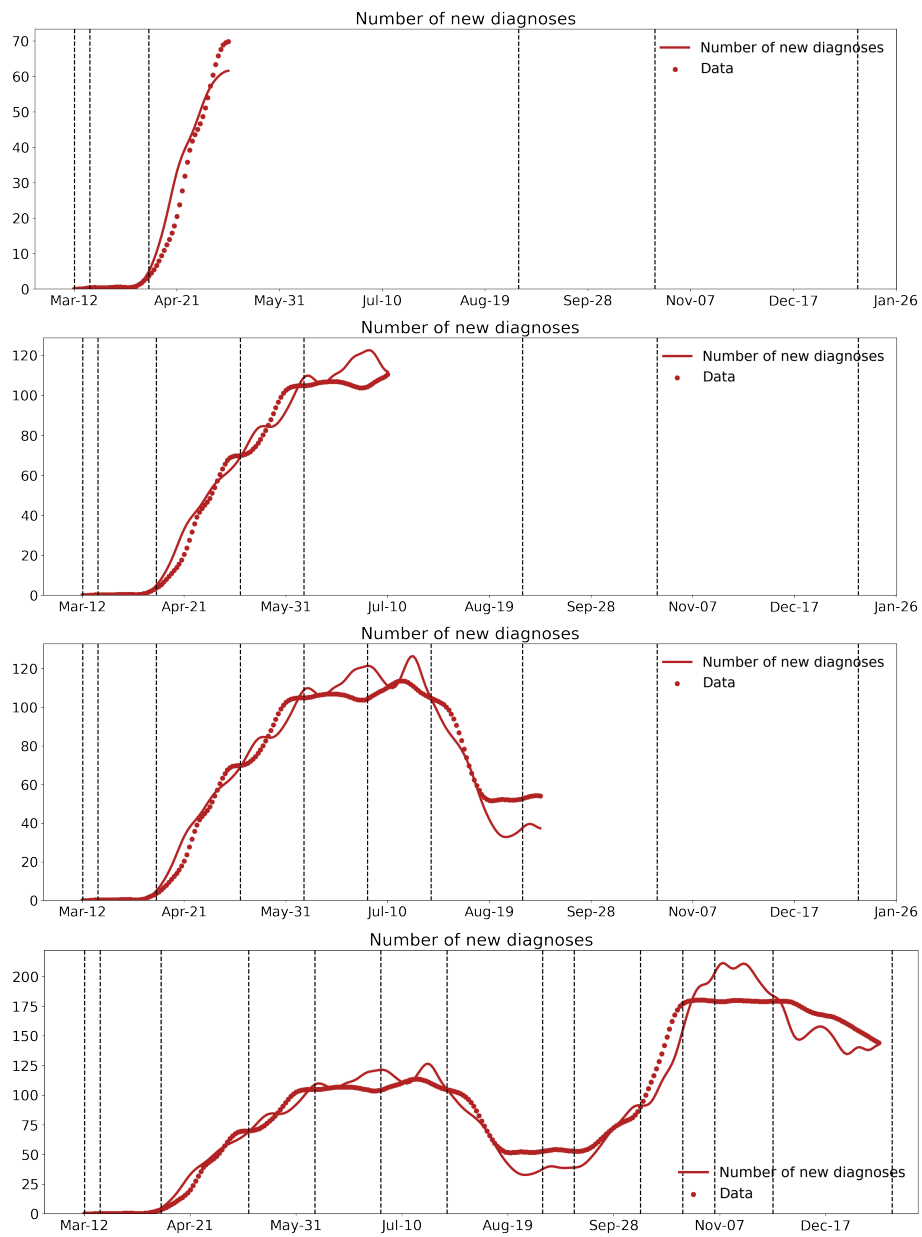


Figure 17: Phased restoration of parameters  $\vec{q}$  using the New Diagnoses dataset from the Novosibirsk region. The vertical dashed lines mark the days when the parameter  $\beta$  changed that were restored from solving an optimization problem.

#### 4. Methods and approaches

Identifying (calibrating) the parameters of an ABM, so that its outputs match observed data, is quite a complex and computation-intensive task due to the large number of the parameters involved. There are different approaches to the problem. In most cases, the parameters are selected manually or one uses averaged experimental results neglecting the specific features of a studied region are used. Analysis of the papers describing epidemiological ABMs has demonstrated that no algorithm could be considered superior for identification of model parameters [24]. According to the paper "...it appears that calibrating individual-based models in epidemiological studies of HIV, malaria and TB transmission dynamics remains more of an art than a science."

In our model, the vector of unknown parameters  $\vec{q}$  was calibrated using the Optuna hyperparameter optimization software [25] to be one of the latest optimizers designed to adjust hyperparameters in machine learning algorithms and neural networks. The optimizer is based on the tree-structured Parzen estimator (TPE) that in many ways is similar to the Bayesian optimizer [26]. However, unlike the Bayesian optimizer that calculates  $p(J(\vec{q})|\vec{q})$ , TPE calculates  $p(\vec{q}|J(\vec{q}))$  and  $p(J(\vec{q}))$  to determine the parameters domain to minimize functional  $J$  by performing Parzen window density estimation, to generate two separate distributions specifying the high - and low-quality regions of the input-space respectively.

The TPE works by ranking the accumulated observations  $\mathcal{D}_K = \{q_k, J(q_k) : k = 1, \dots, K\}$  based on the objective function values. The algorithm selects where  $J$  should be evaluated next by splitting  $\mathcal{D}_K$  into two sets,  $\mathcal{D}_{K_l}^l$  and  $\mathcal{D}_{K_g}^g$  such that  $\mathcal{D}_{K_l}^l$  contains the  $\gamma$ -percentile of the highest quality (i.e. lowest function value) points of  $\mathcal{D}_K$ , whereas  $\mathcal{D}_{K_g}^g$  contains the remaining points. With these definitions, the prior for  $J$  is given by  $P(J < J^\gamma) = \gamma$ . Now, applying non-parametric adaptive parzen windows, two probability distributions  $l(\vec{q})$  and  $g(\vec{q})$  are estimated from  $\mathcal{D}_{K_l}^l$  and  $\mathcal{D}_{K_g}^g$ , respectively. Here,  $l(\vec{q})$  is interpreted as representing the probability of a region in the input space yielding

a high-quality observation while similarly,  $g(\vec{q})$  represents low-quality regions. The likelihood of  $\vec{q}_{K+1}$  belonging to distribution  $l$  and  $g$  may now be expressed by:

$$p(\vec{q}_{K+1}|J(\vec{q})) = \begin{cases} l(\vec{q}), & J(\vec{q}_{K+1}) < J^\gamma, \\ g(\vec{q}), & J(\vec{q}_{K+1}) \geq J^\gamma, \end{cases} \quad (3)$$

where  $J^\gamma$  is the lowest function value found in  $\mathcal{D}_{K_g}^g$ .

The main optimization criterion in the TPE is an expected improvement (EI). According to the definition [27], the EI is a value the function reduces by  
445 at a given moment and can be written as:

$$EI(\vec{q}) = \left( \gamma + \frac{g(\vec{q})}{l(\vec{q})} (1 - \gamma) \right)^{-1} \quad (4)$$

Finally, in order to select a new point to evaluate the objective function at, samples are drawn from  $l(\vec{q})$ , where the sample generating the highest expected improvement is used to evaluate the objective function ( $n_{samp}$ ). A full TPE optimization procedure is described in Algorithm 1.

---

**Algorithm 1** Tree-Parzen estimator optimization

---

**Require:** Parameter values for  $\gamma$ ,  $n_{samp}$  and  $max\_iter$

- 1: **Initialize:** accumulate initial observations
  - 2:  $\mathcal{D}_{init} = \{\vec{q}_k, J(\vec{q}_k), k = 1, \dots, n_{init}\}$
  - 3: **for**  $m=0$  to  $max\_iter$  **do**
  - 4:   Split  $\mathcal{D}_{n_{init}+m}$  to generate  $\mathcal{D}_{m_g}^g, \mathcal{D}_{m_l}^l$
  - 5:   Estimate  $l(\vec{q})$  from  $\mathcal{D}_{n_{init}+m_l}^l$
  - 6:   Estimate  $g(\vec{q})$  from  $\mathcal{D}_{n_{init}+m_g}^g$
  - 7:   Draw  $\vec{q}^s = \vec{q}_k^s : k = 1, \dots, n_{samp}$ , where  $\vec{q}_k^s \sim l(\vec{q})$
  - 8:    $\vec{q}_{m+1} = \operatorname{argmax} EI(\vec{q})$
  - 9:   Evaluate  $J(\vec{q}_{m+1})$
  - 10:   Augment set of observations  $\mathcal{D}_{n_{init}+m} \leftarrow \mathcal{D}_{n_{init}+m+1}$
-

## 450 5. Modeling and forecasting

In this section, we consider mathematical models and scenarios of COVID-19 spread in NY State, (Section 5.2), the UK (Section 5.3) and the Novosibirsk Region (Section 5.4)

### 5.1. Initial datasets

455 To build and analyze the ABMs in the 3 considered regions, the following data were used:

1. Information on population's age distribution according to the local government statistics;
2. Information on the average family size according to the UN data [28];
- 460 3. Statistical data on the people infected with COVID-19, who recovered and died including the number of tests performed that were collected from:
  - The COVID Tracking Project (New York State):  
`https://covidtracking.com/data;`
  - 465 • The official UK Government website for data and insights on Coronavirus (United Kingdom):  
`https://coronavirus.data.gov.uk/;`
  - The RBC website and are available for downloading (Novosibirsk region):  
470 `http://covid19-modeling.ru/data/novosibirsk-region-data.csv.`

For every region, the modeling results for the New Diagnoses, New Deaths and Num Critical (require ICU) datasets were analyzed. In Sections 5.2-5.4 one can find the graphs of 30-day forecasts validated with historical data. The forecasts have an 80% confidence interval to characterize 10% and 90% quantiles. In addition, effective reproduction numbers were calculated for every region.



These numbers indicate how many persons an infectious agent infects on average during the time it has been infectious and calculated as:

$$R(t) = \frac{I_N(t) \cdot f}{I_C(t)}, \quad (5)$$

where  $I_N(t)$  is the number of new infections on day  $t$ ,  $I_C(t)$  is the number of actively infectious people on day  $t$  and  $f$  is the average duration of infectiousness. If  $R(t) < 1$ , the pandemic is considered to stop spreading and keeps spreading otherwise.

### 5.2. COVID-19 spread simulation in NY State

The mismatch (also called error or loss) function (2) for New York State was as follows:

$$J(\vec{q}) = \sum_{t_i=1}^T \left( \frac{|Y_d(t_i) - Y_m(t_i, \vec{q})|}{M_{diag}} + \frac{|D_d(t_i) - D_m(t_i, \vec{q})|}{M_{death}} \right).$$

Here,  $Y_d(t_i)$ ,  $Y_m(t_i, \vec{q})$  are smoothed New Diagnoses with confirmed COVID-19,  $D_d(t_i)$ ,  $D_m(t_i, \vec{q})$  are smoothed New Deaths.

After identification of the parameters, the model was validated with historical data. The New Diagnoses dataset for NY State from 2020.03.02 to 2020.08.31 was taken as model data. The produced forecast covered 50 days and was compared against statistical data for the given test period (2020.09.01 — 2020.10.20). The modeling results can be seen in Fig. 18.

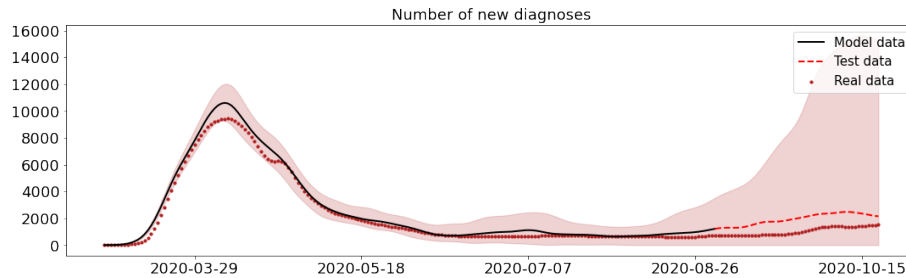


Figure 18: Forecast for New Diagnoses validated with historical data for NY State. The black line displays the modeled period, and the red dots – the New Diagnoses dataset.

Despite the size of the confidence interval that started to increase from  
485 2020.09.01, the increment rate of New Diagnoses was close to the test data.

Figure 19 presents the results of a 30-day forecast with restored vector of unknown parameters for NY State, where the dots mark the real data accumulated from 2020.03.02 to 2021.03.01. The forecast for New Diagnoses assumed the rate of daily tests remained unchanged.

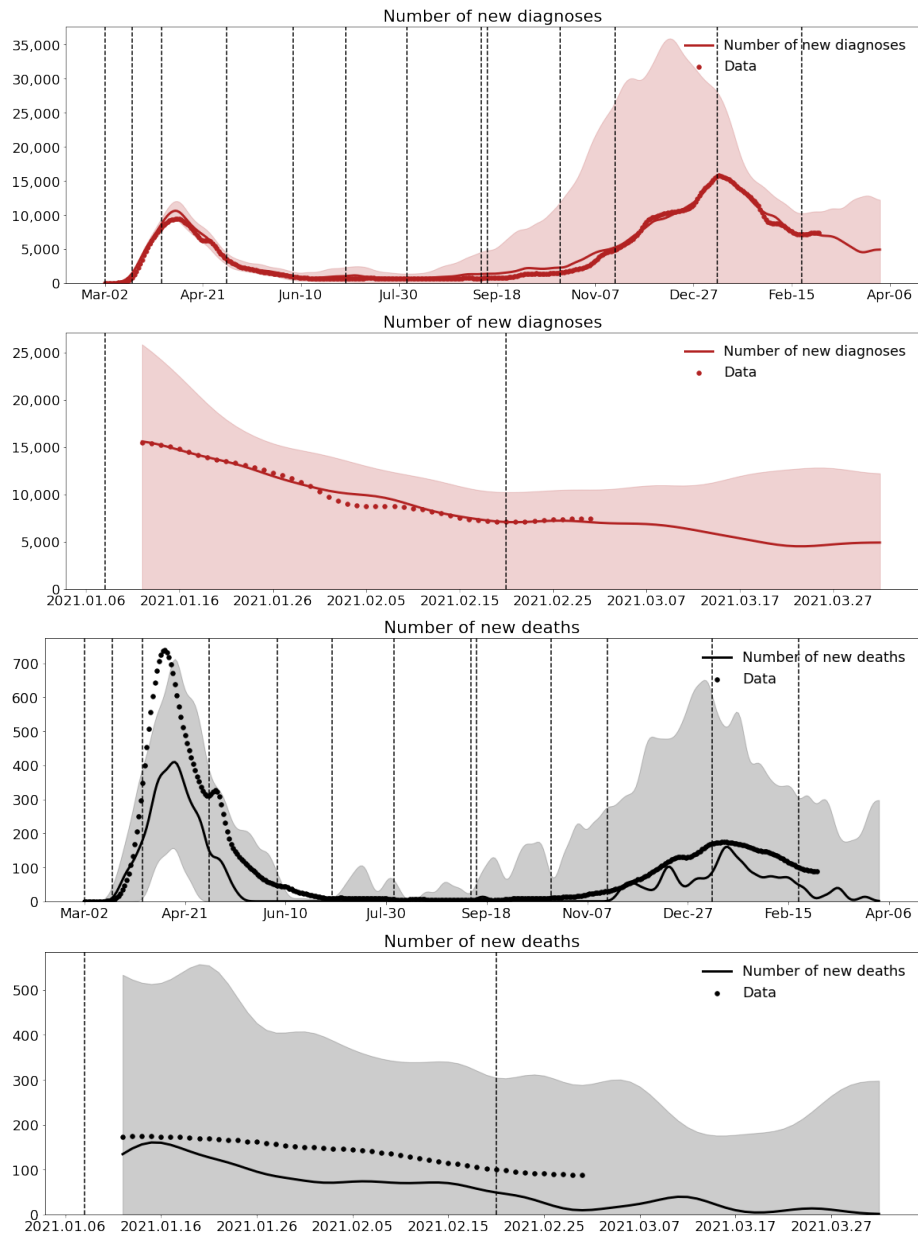


Figure 19: Model calibration results for 10 simulations + a 30-day forecast for New Diagnoses (two top graphs) and New Deaths (two bottom graphs) in NY State. The shaded areas are 10% and 90% quantiles, the solid line – the median value of modeling result, and dots – real data. The dashed vertical lines are COVID-19 containment measures.

490 The effective reproduction number  $R(t)$  calculated by (5) showed the pandemic began its downturn in NY State in January 2021.

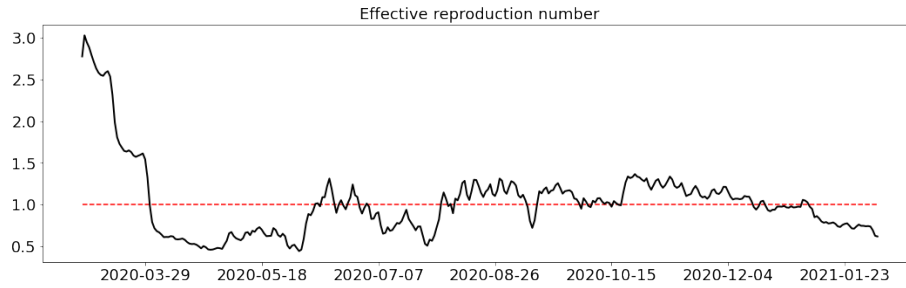


Figure 20: Effective reproduction number  $R(t)$  for the New York State. The red dashed line marks  $R(t) = 1$ .

### 5.3. COVID-19 spread simulation in the UK

The mismatch function (2) for United Kingdom was as follows:

$$J(\vec{q}) = \sum_{t_i=1}^T \frac{|Y_d(t_i) - Y_m(t_i, \vec{q})|}{M_{diag}}$$

Here  $Y_d(t_i)$ ,  $Y_m(t_i, \vec{q})$  are smoothed New Diagnoses with confirmed COVID-19.

Firtly, the parameters that minimizing mismatch function were identified.

495 The New Diagnoses dataset for the UK from 2020.02.07 to 2020.08.31 was taken as model data. The produced forecast covered 50 days and was compared against observed data for the given test period (2020.09.01 – 2020.10.20). The modeling results can be seen in Fig. 21. It is noteworthy that the prediction error after comparing with real data was only 1.2%.

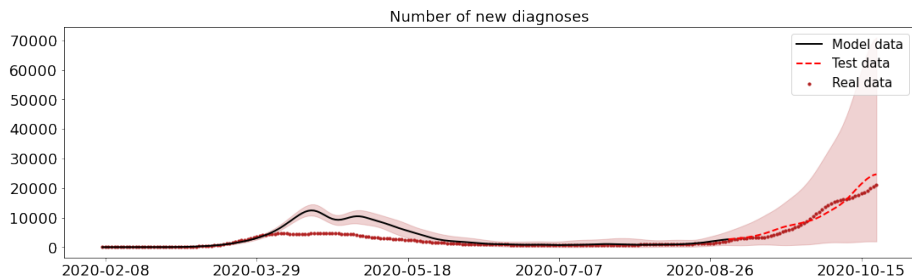


Figure 21: Forecast for New Diagnoses validated with historical data for UK. The black line displays the modeled period, and the red dots – the New Diagnoses dataset. The red dashed line marks the test period.

500 Figure. 22 presents the results of a 30-day forecast for the UK with restored vector of unknown parameters  $\vec{q}$  as is described in Section 4. The forecast for New Diagnoses assumed the rate of daily tests remained unchanged.

As for New Deaths, the modeling results differed from the real data by 50%, which was related to the target functional  $J(\vec{q})$  that contained information only  
 505 about New Diagnoses, while the error for this indicator was comparable to that of New Deaths. To reduce the error, weighed information about the New Deaths indicator is to be added in the functional. The problem of determining the weight coefficients needs further consideration.

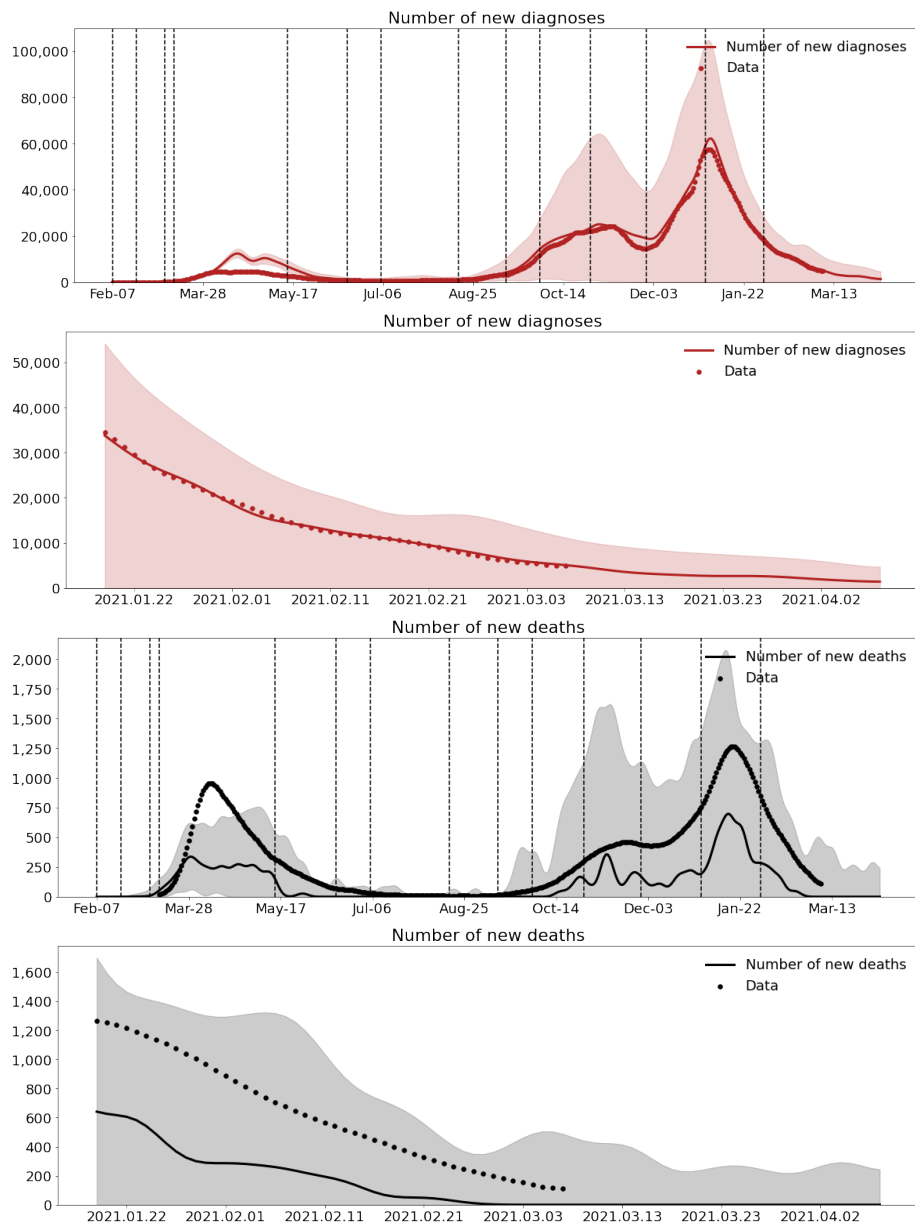


Figure 22: Model calibration results for 10 simulations + a 30-day forecast for New Diagnoses and New Deaths in the UK. The shaded areas are 10% and 90% quantiles, the solid line – the median value of modeling result, and dots – real data. The dashed vertical lines are COVID-19 containment measures.

The effective reproduction number  $R(t)$  calculated by (5) for a time period

510 from 2020.02.07 to 2021.03.01 in the UK can be seen in Fig. 23. The graph demonstrates the UK had a second infection wave in fall 2020 and in January 2021, after which the pandemic began its downturn.

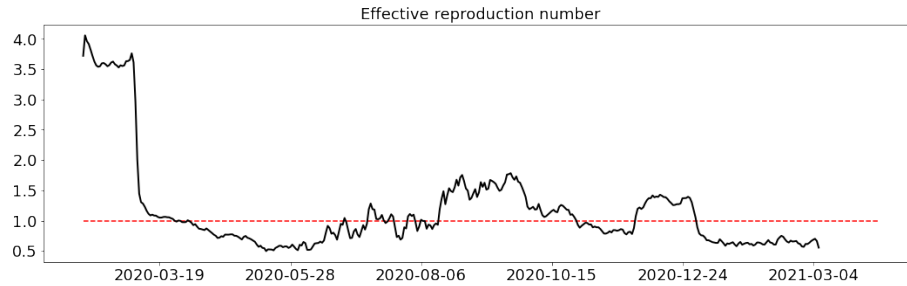


Figure 23: Effective reproduction number  $R(t)$  for the UK. The red dashed line marks  $R(t) = 1$ .

#### 5.4. COVID-19 spread simulation in the Novosibirsk region

The mismatch function (2) for Novosibirsk region was as follows:

$$J(\vec{q}) = \sum_{t_i=1}^T \frac{|Y_d(t_i) - Y_m(t_i, \vec{q})|}{M_{diag}}.$$

Here  $Y_d(t_i)$ ,  $Y_m(t_i, \vec{q})$  are smoothed New Diagnoses with confirmed COVID-19.

515 The New Diagnoses dataset for validation model in the Novosibirsk region was from 2020.03.12 to 2020.11.01. The produced forecast covered 45 days and was compared against statistical data for the given test period (2020.11.02 – 2020.12.15). The modeling results shown in Fig. 24 demonstrated that preserv-  
 520 the spread by more than 25%. This difference between modeling and real data was due to the data space’s stationarity (see Section 2.2.2) amid unaccounted administrative measures.

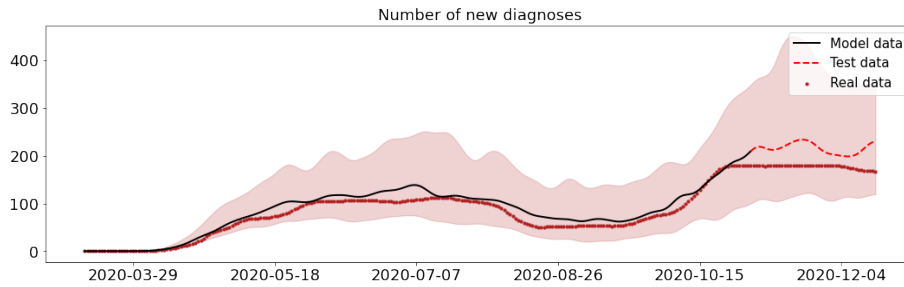


Figure 24: Forecast for New Diagnoses validated with historical data for the Novosibirsk region. The black line displays the modeled period, and the red dashed line – the test period. The red dashed line marks the test period. The shaded areas are 10% and 90% quantiles for 10 simulations

Figure 25 presents the results of a 30-day forecast for the Novosibirsk region with a restored vector of unknown parameters  $\vec{q}$  as is described in Section 4.

525 The colored dots mark the real data (to 2021.02.15) that were used to solve the inverse problem; the black ones (2021.02.16 – 2021.03.01) – to test the forecast. The forecast for New Diagnoses assumed the rate of daily tests remained unchanged. It is noteworthy that despite the forecast error for the New Diagnoses indicator participating in the minimization of target functional  $J(\vec{q})$  was 10%,

530 the forecast error for Num Critical did not exceed 5%.



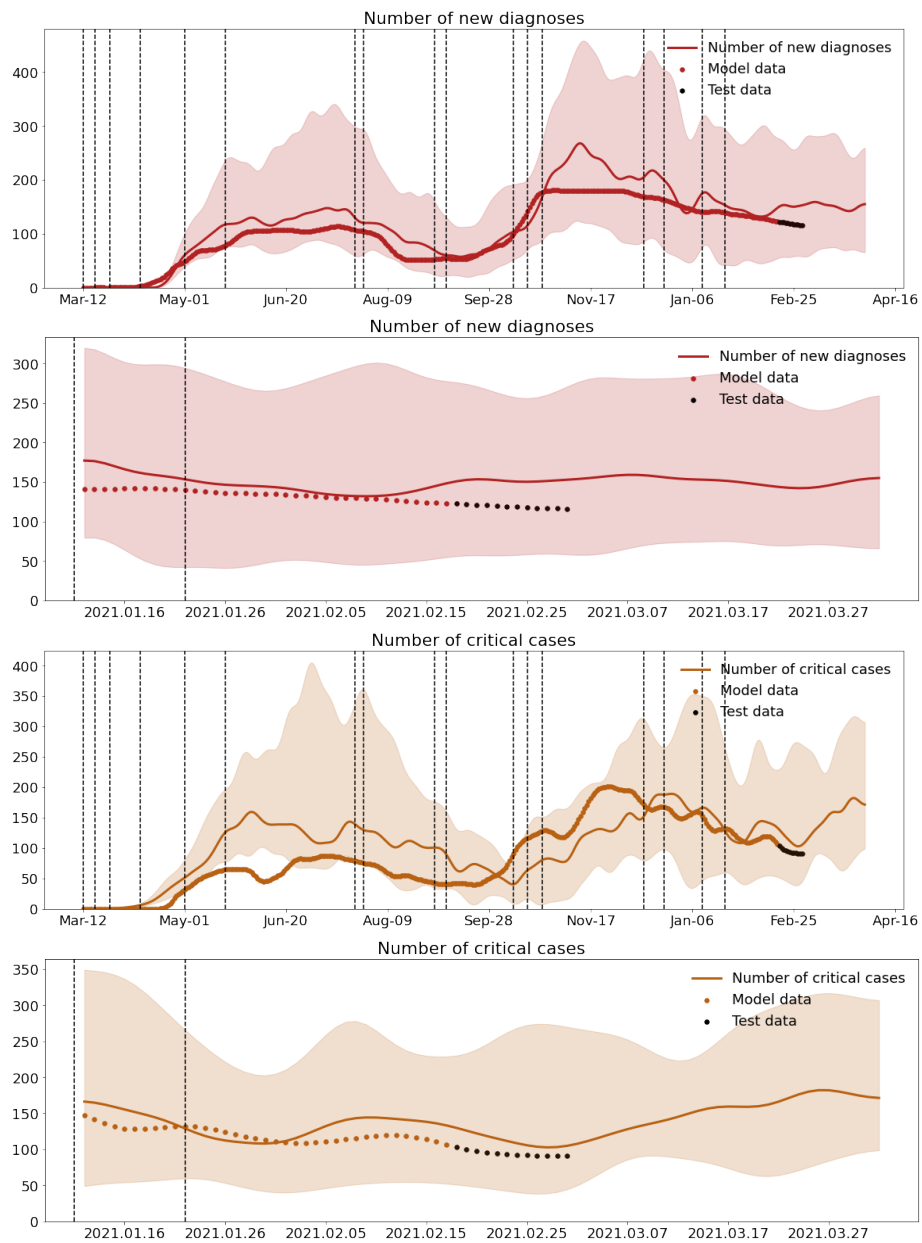


Figure 25: Model calibration results for 10 simulations + a 30-day forecast for New Diagnoses and Num Critical in the Novosibirsk region. The shaded areas are 10% and 90% quantiles, the solid line – the median value of modeling result, and dots – real data. The dashed vertical lines are COVID-19 containment measures.

The effective reproduction number  $R(t)$  calculated by (5) for a time period from 2020.03.12 to 2021.02.01 in the Novosibirsk region can be seen in Fig. 26. The graph demonstrates the pandemic had been under control since the end of 2020.

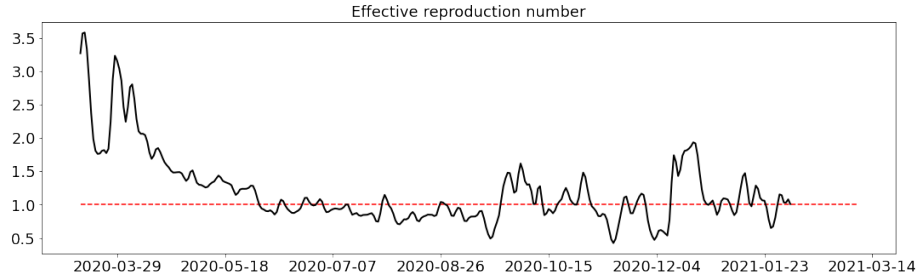


Figure 26: Effective reproduction number  $R(t)$  for the Novosibirsk region. The red dashed line marks  $R(t) = 1$ .

535 **6. Conclusions and discussions**

Mathematical models are effective tools to deal with the time evolution and patterns of disease outbreaks. They provide us with useful predictions in the context of the impact of intervention in decreasing the number of infections and deaths.

540 This paper provides a detailed analysis of the statistical data, including the number of tested, positive, mortality, hospitalization and critical cases, on COVID-19 spread in NY State, the UK and the Novosibirsk region and presents a solution to the problem of identification of unknown epidemiological parameters (transmissibility; the initial number of infected individuals; probability of being tested, etc.) in an ABM. The problem has been considered as the mini-  
 545 mization of a target functional in relation to daily numbers of tested, positive and mortality cases in the studied regions and become an important modification of the Covasim package [21]. The minimization problem has been solved using the Optuna hyperparameter optimization software and the Parzen esti-

550 mation method. Normal gradient descent methods do not work with Covasim  
or other agent-based models, due to the stochastic variability between model  
runs that makes the landscape very “bumpy” (i.e., many transient local min-  
ima). One way of getting around this is to perform many different runs and  
take the average. However, averaging over many runs is computationally ex-  
555 pensive, since running  $N$  simulations of ABM will only reduce the noise by  
 $\sqrt{N}$  [23].

The results of data analysis in every studied region showed the weekly sea-  
sonality of New Tests, which helped us forecast the future values of this time  
series. It worth noting that some countries have their own rules of statistical  
560 analysis that have to be accounted for when carrying out modeling, e.g. in  
the USA, the New Diagnoses indicator contains a certain percentage of prob-  
able cases, while New Deaths in the UK accounts for all the deaths that have  
occurred within 28 days since a positive COVID-19 test, even if such death has  
not been provoked by the virus.

565 Due to the high sensitivity of the transmissibility parameter  $\beta$ , the accuracy  
of its identification becomes crucial for uncovering the pattern of COVID-19  
spread in an investigated region. However, not all containment measures af-  
fect the pattern. For that reason, when developing an ABM calibration algo-  
rithm based on epidemiological data, we paid special attention to transmissi-  
570 bility and the times this parameter changed while modeling. These character-  
istics were determined from solving the minimization problem as a piecewise  
- constant function, while solving the inverse problem restored the parameter  
together with its times of change.

The devised ABM has been validated with historical data from 2020. The  
575 modeling results for the three regions in question have demonstrated that pre-  
serving the introduced containment measures would have sustained New Di-  
agnoses in NY State and the Novosibirsk region during March 2021 and would  
have reduced them in the UK.

Due to the specific features of the observed data in the Novosibirsk region,  
580 where two time series are stationary with probability of 1, the model’s forecast

accuracy has been lower for new cases of infection and more accurate for cases of hospitalization, e.g., the confidence interval values for the new case of infection registered daily was [70; 270] individuals and for hospitalizations - [90; 300] individuals, both including as model solutions as real data.

585 The proposed agent-based model has the following limitations. We do not fix population number changing during model year, consider waning of immunity to coronavirus, or the possibility of re-infection. We also use more simplistic contact structures than in real life.

Our future plans are investigation of model identifiability to real data and  
590 sensitivity analysis. It will also be necessary to investigate the influence of vaccination on COVID-19 propagation.

## 7. Competing interests statement

The authors declare that they have no known competing financial interests or personal relationships that could have appeared to influence the work reported in this paper.  
595

## 8. Acknowledgements

The data analysis part (section 2) is supported by the Russian Foundation for Basic Research and Royal Society (project no. 21-51-10003). The agent-based mathematical model construction and analysis of numerical results (sections 3,  
600 4, 5) was supported by the Russian Science Foundation (project no. 18-71-10044) and the Royal Society *IEC\R2\202020* – International Exchanges 2020 Cost Share between UK and Russia. Authors would like to thank Professor Sergey Kabanikhin and Doctor Alexey Romanyukha for the problem analysis and fruitful discussions. Also we would like to thank Yan Reznichenko for  
605 language help.

## References

- [1] I.Cooper, A.Mondal and C.G. Antonopoulos: A SIR model assumption for the spread of COVID-19 in different communities. *Chaos, Solitons and Fractals* **139**(110057) (2020)
- 610 [2] F. Ndairoua I. Area, J.J.Nieto and D.F.M.Torres: Mathematical modeling of COVID-19 transmission dynamics with a case study of Wuhan. . *Chaos, Solitons and Fractals* **135**(109846) (2020)
- [3] Kai D., Goldstein G.F., Morgunov A., Nangalia V., Rotkirch A.: Universal masking is urgent in the COVID-19 pandemic: SEIR and agent-based  
615 models, empirical validation, policy recommendations. *arXiv preprint arXiv:2004.13553*. (2020). 10.13140/RG.2.2.21662.08001
- [4] Wolfram C.: An Agent-Based Model of COVID-19. *Complex Systems* **29**(1), 87-105 (2020). 10.25088/ComplexSystems.29.1.87.
- [5] Cuevas E.: An agent-based model to evaluate the COVID-19 transmission risks in facilities. *Computers in biology and medicine* **121**(103827) (2020).  
620 <https://doi.org/10.1016/j.compbimed.2020.103827>.
- [6] Chang S., Pierson E., Koh P.W., Gerardin J., Redbird B., Grusky D., Leskovec J.: Mobility network models of COVID-19 explain inequities and inform reopening *Nature* **589**, 82–87 (2021).  
625 <https://doi.org/10.1038/s41586-020-2923-3>.
- [7] Silva P.C.L., Batista P.V.C., Lima H.S., Alves M.A., Guimarães F.G., Silva R.C.P.: COVID-ABS: An agent-based model of COVID-19 epidemic to simulate health and economic effects of social distancing interventions. *Chaos, Solitons and Fractals* **139**(110088), (2020).  
630 <https://doi.org/10.1016/j.chaos.2020.110088>
- [8] Mellacher P.: COVID-Town: An integrated economic-epidemiological agent-based model. *Munich Personal RePEc Archive Paper No. 103661*, (2020).

- [9] Tracking Coronavirus in New York: Latest Map and Case Count <https://www.nytimes.com/interactive/2021/us/new-york-covid-cases.html>  
635
- [10] RBC site - coronavirus statistics in Novosibirsk region: <https://nsk.rbc.ru/>
- [11] The COVID Tracking Project in USA: <https://covidtracking.com/data>
- 640 [12] Hodrick R.J., and Edward C. P.: "Postwar U.S. Business Cycles: An Empirical Investigation." *Journal of Money, Credit and Banking*, vol. 29, no. 1, pp. 1–16. (1997)
- [13] Bartolucci F., Cardinali A., Pennoni F.: A Generalized Moving Average Convergence/Divergence for Testing Semi-strong Market Efficiency.  
645 *Mathematical and Statistical Methods for Actuarial Sciences and Finance*. 10.1007/978-3-319-89824-7\_18. (2018).
- [14] Grimstad, B. and Knudsen, B.R. Mathematical programming formulations for piecewise polynomial functions. *J Glob Optim* 77, 455–486 (2020).
- [15] Coronavirus (COVID-19) in the UK: <https://coronavirus.data.gov.uk/>  
650
- [16] Dabral P.P. and Murry, M.Z.: Modelling and forecasting of rainfall time series using SARIMA. *Environ. Process.* 4, 399–419 (2017).
- [17] Balasmeh O., Babbar R. and Karmaker T.: Trend analysis and ARIMA modeling for forecasting precipitation pattern in Wadi Shueib catchment area in Jordan. *Arab J Geosci* (2019).  
655
- [18] Box G.E.P. and Cox D.R.: An analysis of transformations. (With discussion). *J. Roy. Statist. Soc. Ser. B* 26, 211–252 (1964).
- [19] Williams, T. Adaptive Holt—Winters Forecasting. *J Oper Res Soc* 38, 553–560 (1987).

- 660 [20] Kerr C., Stuart R., Mistry D., Abeysuriya R., Hart G., Rosenfeld K., Selvaraj P., Nunez R., Hagedorn B., George L., Izzo A., Palmer A., Delpont D., Bennette C., Wagner B., Chang S., Cohen J., Panovska-Griffiths J., Jastrzebski M., Oron A., Wenger E., Famulare M. and Klein D.: Covasim: an agent-based model of COVID-19 dynamics and interventions. *Medverix* (2020).  
665 10.1101/2020.05.10.20097469.
- [21] Kerr C., Rosenfeld K., Hagedorn B., Mistry D. and Klein D.: COVID-19 trends in Oregon: Preparing for opening up. *Institute for Disease Modeling* (2020).
- [22] Kerr C., Hagedorn B., Mistry D. and Klein D.: COVID-19 trends in Oregon: Implications for interventions. *Institute for Disease Modeling* (2020).  
670
- [23] Covasim documentation: <https://docs.idmod.org/projects/covasim/en/latest/index.html>
- [24] C.M. Hazelbag, J. Dushoff, E.M. Dominic, Z.E. Mthombothi and W.Delva: Calibration of individual-based models to epidemiological data: A systematic review. *PLOS Computational Biology* (2020).  
675
- [25] OPTUNA: hyperparameter optimization framework: <https://optuna.org/>
- [26] Rasmussen C.E. and Williams C.K.I.: Gaussian Processes for Machine Learning (2006).
- 680 [27] J.Bergstra and R.Bardenet, Y.Bengio et al.Advances in Neural Information Processing Systems. *Curran Associates Incorporation*. **24** (2011)
- [28] Household Size, 2019, UN. <https://population.un.org/Household/#/countries/840>